Preprints of the 19th World Congress
The International Federation of Automatic Control
Cape Town, South Africa. August 24-29, 2014

Model accuracy impacts for active damping of a viscoelastic beam

Hans Norlander *

* *Systems and Control, Department of Information Technology, Uppsala University, Sweden (e-mail: hans.norlander@it.uu.se)*

Abstract: This study concerns the effect of model accuracy on closed loop performance for active damping of vibrations. The system, a viscoelastic cantilever beam, is represented by Euler-Bernoulli beam equations. Standard LQG is used for control design, requiring finite order models. Two such models are produced, one based on truncated modal analysis, and one based on numerical fit of the frequency response. It is found that all controllers stabilize the system and attenuates vibrations, but controllers based on the numerically fitted model perform notably better than those based on truncated modal analysis.

Keywords: Mechanical systems; vibration control; LQG control; smart structures; frequency response data; model approximation

1. INTRODUCTION

In automatic control there are two assertions that are often stated as being true, and usually taught to students in the introductory control course already. The first "truth" is: "the better model, the better performance of the closed loop system". The second "truth" is: "feedback allows a good performance in spite of model errors/uncertainties". Although these two statements do not exclude each other — they both are really true in many senses — they do somehow point in opposite directions concerning the requirements on the model.

The purpose of the present study is to test these two assertions for a more demanding control problem. The control objective is to suppress vibrations in a viscoelastic cantilever beam actuated by piezoelectric elements. The physical model of such a beam is a distributed parameter system, *i.e.* it is governed by partial differential equations (PDEs). However, almost all model based controller design techniques are based on models expressed as ordinary differential equations (ODEs) of finite order. From that perspective PDEs are usually considered as being of infinite order. In order to enable the use of such controller design techniques any PDE model must be approximated by some finite order ODE. In this work two different low order models of the cantilever beam are used for control design, and the corresponding closed loop systems are compared and evaluated. The two models are reflecting the two assertions mentioned above, in the following sense: The first model is made to have its frequency response as close as possible to that of the true system. The second model is obtained with the aid of a rather "simple" (not theoretically, but in practice) but physically motivated approach, with only minor adjustments to match the frequency response of the true system, and thus resulting in a more "rough" model.

The paper is organised as follows. In Section 2 the Euler-Bernoulli beam equation is presented. This is a PDE, and in Section 3 it is used to derive the theoretical, physical model of the beam. This theoretical model is then regarded as the true system to be used in comparisons and evaluations of the obtained models and controllers. In Section 4 the two methods for obtaining finite order models of the true system are presented, and the resulting models are compared to the true system. The two models are then used for controller design in Section 5, where the standard LQG technique is used in a straightforward manner. In Section 6 the different controllers are applied to the true system and the corresponding closed loop systems are compared and evaluated.

2. THE EULER-BERNOULLI BEAM

The simplest distributed model for describing bending vibrations in an elastic beam is the Euler-Bernoulli beam equation (E-B equation), see *e.g.* Meirovitch (1997):

$$\frac{\partial^2}{\partial x^2}\left(EI\frac{\partial^2}{\partial x^2}w(t,x)\right)+\rho A\frac{\partial^2}{\partial t^2}w(t,x)=f(t,x). \qquad (1)$$

Here $w(t,x)$ is the vertical deflection of the centerline of the beam at time t and in the point x, see Figure 1. Furthermore, ρ is the density, and A is the cross-section area of the beam. The product EI represents the bending stiffness (E is the Young's modulus of elasticity and I is the area moment of inertia about the normal of the x-z-plane as in Figure 1), which in general depends on x. In simple cases, like here, EI is piecewise constant (w.r.t. x), turning the two second order partial derivatives in (1) into one fourth order partial derivative with respect to x. In (1) $f(t,x)$ represents the distribution of external forces acting on the beam. Cases in which these forces are distributed pointwise, like the force $F(t)$ in Figure 1, may be handled in different ways. One possibility is to let $f(t,x)$ be a sum of Dirac's delta functions. This is used in the derivation of the model structure in Section 4.2. Another way is to set $f(t,x)\equiv 0$, and to let the external forces enter the system in terms of boundary and compatibility conditions. This approach is used in the remaining part of this section and in Section 3.

A simple way of solving (1) is to utilize the Fourier transform (w.r.t. time), and to solve the resulting ODE. This also offers a convenient way of taking damping into account.

As described above, the basic form (1) of the E-B equation is valid for an elastic beam, *i.e.* the beam is totally undamped, and this is due to the idealizations and simplifications used in the derivation of (1). However, all real beams are more or less damped, and in a more realistic treatment it is sometimes relevant to take this damping into account. For viscoelastic materials damping may be accounted for by letting the Young's modulus of elasticity be complex-valued and frequency dependent, and this is then referred to as the *complex modulus* — see *e.g.* Hillström (2001) and the references therein.

Introduce the notation $\hat{s}(\omega)$ for the Fourier transform of a generic signal $s(t)$, and let $E(\omega)$ denote the complex modulus. The Fourier transformed version of the E-B equation is then

$$E(\omega)I\frac{d^4}{dx^4}\hat{w}(\omega,x) - \omega^2\rho A\hat{w}(\omega,x) = 0, \qquad (2)$$

i.e. an ODE in x. The solutions of (2) are

$$\hat{w}(\omega,x) = r^T(\omega,x)c(\omega) \qquad (3)$$

where $r^T(\omega,x) = \begin{bmatrix} e^{\lambda_1 x} & e^{\lambda_2 x} & e^{\lambda_3 x} & e^{\lambda_4 x}\end{bmatrix}$ and $c(\omega) = \begin{bmatrix}\alpha(\omega) & \beta(\omega) & \gamma(\omega) & \delta(\omega)\end{bmatrix}^T$. Here λ_k, $k = 1,\dots,4$ are the roots of the characteristic equation,

$$E(\omega)I\lambda^4 - \omega^2\rho A = 0 \;\Leftrightarrow\; \lambda_k = i^{k-1}\left(\omega^2\frac{\rho A}{E(\omega)I}\right)^{\frac{1}{4}}, \qquad (4)$$

where $i = \sqrt{-1}$. Although not spelled out explicitly here it is understood that $\lambda_k = \lambda_k(\omega) \in \mathbb{C}$ for $k = 1,\dots,4$, *i.e.* they are frequency dependent and complex-valued.

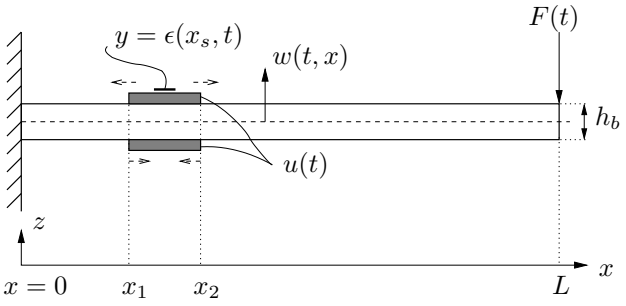

Fig. 1. Cantilever beam with piezoelectric elements (shaded).

3. THE DISTRIBUTED MODEL

The system under consideration in this study is a cantilever beam, as depicted in Figure 1, *i.e.* the beam is clamped at one end and free at the other end. The beam, which has a rectangular cross-section, is made of a viscoelastic material, and it has two piezoelectric elements attached onto it. These are placed at the same x-position but at opposite sides of the beam, and are used as actuators. By putting an electric voltage over them they will tend to expand or contract, and thereby generate a bending moment on the beam. The voltage over the piezoelectric elements (the same over both elements, but with opposite signs) is the input to the system. The beam is also affected by a disturbance force, $F(t)$ in Figure 1, acting in the z-direction at the free end of the beam (at $x = L$).

The system is modeled using the Fourier transformed E-B equation (2). In order to handle the effect of the piezoelectric elements, the beam is split spatially into three segments along the x-axis, with interfaces in x_1 and x_2 according to Figure 1. Each segment is governed by an equation (2). The properties of the beam are listed in Table 1.

Entity	Notation	Value
Beam length [m]	L	0.59
Beam width [m]	b	0.01
Beam thickness [m]	h_b	0.002
Beam density [kg/m^3]	ρ_b	1183
Piezo. length [m]	$x_2 - x_1$	0.0318
Piezo. thickness [m]	h_p	0.00066
Piezo. density [kg/m^3]	ρ_p	7878
Piezo. Young's modulus [N/m^2]	E_p	$5.70 \cdot 10^{10}$
Piezo. position [m]	x_1	0.202

Table 1. Properties of the beam and the piezoelement.

The complex modulus of the viscoelastic material is modeled using a so called standard linear solid model (see Hillström (2001))

$$E_b(\omega) = \frac{M_R}{2}\left(\frac{1+i\omega\tau_{\epsilon 1}}{1+i\omega\tau_{\sigma 1}} + \frac{1+i\omega\tau_{\epsilon 2}}{1+i\omega\tau_{\sigma 2}}\right),$$

where $M_R = 4.029 \cdot 10^9$ [N/m^2], and the time constants

$$\tau_{\epsilon 1} = 4.369 \cdot 10^{-3},\;\; \tau_{\sigma 1} = 2.954 \cdot 10^{-3},$$
$$\tau_{\epsilon 2} = 450.9 \cdot 10^{-6},\;\; \tau_{\sigma 2} = 365.8 \cdot 10^{-6},$$

all in [s]. These values were experimentally determined in Hillström et al. (2003).

The system is described by three fourth order ODEs (one for each segment),

$$[E(\omega)I]_k\frac{d^4}{dx^4}\hat{w}_k(\omega,x) - \omega^2\,[\rho A]_k\,\hat{w}_k(\omega,x) = 0 \qquad (5)$$

for $k = 1,2,3$, so that

$$\hat{w}(\omega,x) = \hat{w}_1(\omega,x) \;\text{ for }\; 0 < x < x_1,$$
$$\hat{w}(\omega,x) = \hat{w}_2(\omega,x) \;\text{ for }\; x_1 \le x \le x_2$$
$$\text{and }\; \hat{w}(\omega,x) = \hat{w}_3(\omega,x) \;\text{ for }\; x_2 < x \le L.$$

The deflections $\hat{w}_k(\omega,x)$, $k = 1,2,3$, are coupled by the boundary conditions

$$\hat{w}_1(\omega,0) = 0, \quad \frac{d}{dx}\hat{w}_1(\omega,0) = 0,$$
$$\hat{M}_3(\omega,L) = 0, \quad \hat{T}_3(\omega,L) = -\hat{F}(\omega), \qquad (6)$$

and the compatibility conditions

$$\hat{w}_k(\omega,x_k) = \hat{w}_{k+1}(\omega,x_k),\;\; \frac{d\hat{w}_k}{dx}(\omega,x_k) = \frac{d\hat{w}_{k+1}}{dx}(\omega,x_k),$$
$$\hat{M}_k(\omega,x_k) = \hat{M}_{k+1}(\omega,x_k),\;\; \hat{T}_k(\omega,x_k) = \hat{T}_{k+1}(\omega,x_k), \qquad (7)$$

for $k = 1,2$. Here $\hat{M}_k(\omega,x)$ is the bending moment and $\hat{T}_k(\omega,x)$ is the transversal force. The control input, *i.e.* the voltage $\hat{u}(\omega)$ applied to the piezoelectric elements, enters the system through $\hat{M}_2$ (see Norlander (2011)), and the disturbance force $\hat{F}(\omega)$ enters through $\hat{T}_3$, as seen from (6). Since every $\hat{w}_k(\omega,x)$ is governed by its corresponding ODE (5), with solution in accordance with (3), we have

$$\hat{w}_k(\omega,x) = r_k^T(\omega,x)c_k(\omega), \qquad (8)$$

where $r_k^T(\omega,x)$ is determined by the corresponding characteristic equation (4), and $c_k(\omega)$, $k = 1,2,3$, are determined jointly from the boundary and compatibility conditions (6) and (7). The deflection depends linearly (affine) on the external inputs, the control signal $\hat{u}(\omega)$ and the disturbance force $\hat{F}(\omega)$, *i.e.*

$$\hat{w}(\omega,x) = \hat{H}^u(\omega,x)\hat{u}(\omega) + \hat{H}^F(\omega,x)\hat{F}(\omega). \qquad (9)$$

A derivation of (9) is found in Norlander (2011).

In this study it is not the deflection, w, but rather the strain, ϵ, that is measured, by a strain gauge. In contrast to the actuators, *i.e.* the piezoelectric elements, the strain gauge is very small and light and its influence on the beam is considered negligible. Therefore it is neglected in the model.

The strain is related to the deflection according to $\hat{\epsilon}(\omega, x) = -\frac{h(x)}{2}\frac{d^2}{dx^2}\hat{w}(\omega, x)$, where $h(x)$ is the thickness of the beam at position x. The strain gauge is placed on top of one of the piezoelectric elements, at $x_s = (x_1 + x_2)/2$. The measured strain is thus $y(t) = \epsilon(x_s, t)$, and it is regarded as the output of the system.

From input to output the system is described by

$$\hat{y}(\omega) = \hat{G}^u(\omega)\hat{u}(\omega) + \hat{G}^F(\omega)\hat{F}(\omega), \tag{10}$$

where

$$\hat{G}^\alpha(\omega) = -\frac{h(x_s)}{2} \cdot \frac{d^2}{dx^2}\hat{H}^\alpha(\omega, x_s), \quad \alpha = u, F.$$

In this study two different ways of finding approximate, low order models for model based control design are used. For this reason the coupled ODEs (5), together with the boundary and compatibility conditions (6) and (7) etc, finally resulting in (10), are regarded as a reference and are referred to as the *true system*.

4. FINITE ORDER MODELS

Two methods for obtaining low order models will be compared here. Method 1 is a rather ad hoc approach, while Method 2 is based on modal analysis of the E-B equation (1). The system is very resonant, and as it is of infinite order there are infinitely many resonant modes; see Figure 2. The purpose of feedback control of this beam is to dampen the vibrations due to these resonances, and in particular the vibrations caused by a disturbance force acting on the tip of the beam, at $x = L$ as shown in Figure 1. However, any implementable controller must be of finite order, implying that only a finite number of the resonances can be attenuated. As is apparent from the Bode plot from F to y, the right graph in Figure 2, the resonance peaks are decreasing with increasing frequency. Therefore it seems reasonable to try to suppress the first few peaks — that would have the biggest impact. This also indicates that the model used in the control design should have a good fidelity in a frequency range covering at least the resonant modes of interest. In this study the ambition is to suppress the first three resonance peaks.

Due to the resonant nature of the beam, both methods used here are based on model representations in form of sums of second order systems with a small damping ratio, were every term represents one resonant mode/peak. Let $G_n^u(s, \theta_j^u)$ and $G_n^F(s, \theta_j^F)$ denote the approximate, finite order models of $\hat{G}^u(\omega)$ and $\hat{G}^F(\omega)$ respectively. The index n indicates the number of modes in the models (*i.e.* the order of the models is $2n$), while θ_j^u and θ_j^F represents the parameter vectors for the model from method $j = 1, 2$. This means that

$$G_n^F(s, \theta_j^F) = \sum_{k=1}^{n} \frac{\psi_{j,k}}{s^2 + 2\zeta_{j,k}\omega_{j,k}s + \omega_{j,k}^2}, \tag{11}$$

where $\psi_{j,k}, \omega_{j,k}, \zeta_{j,k} \in \mathbb{R}$, $k = 1, \ldots, n$, are the elements of θ_j^F (and likewise for $G_n^u(s, \theta_j)$). (The index j indicates which method that is used — for brevity it is omitted in the sequel.)

4.1 Method 1

The idea behind method 1 is to have the frequency response of the model as close as possible to the true system, in the frequency range of interest. In this sense method 1 is equivalent to the "Ad-hoc Approach" presented in Nauclér et al. (2005), where the criterion

$$V(\theta) = \sum_{m=1}^{N} \left|\hat{G}(\omega_m) - G_n(i\omega_m, \theta)\right|^2 W(\omega_m) \tag{12}$$

is (numerically) minimized. Here $W(\omega_m)$ is a frequency-dependent weight, and $G_n(s, \theta)$ is a rational function with arbitrary but predefined degrees of the numerator and denominator polynomials. In this study the model is obtained in two steps.

Motivated by the proposed structure in (11), the first step is to model each mode

$$\gamma_k(s) = \frac{1}{s^2 + 2\zeta_k\omega_k s + \omega_k^2}, \;\; k = 1, \ldots, n,$$

i.e. to determine the natural frequency ω_k and the damping ratio ζ_k of each mode. This is easily performed with the criterion (11) in a narrow frequency interval containing the peak corresponding to the mode k. In this first step no account is made for the order of the sought model — each mode is modeled individually.

Given the individual modes the model can be parameterized as

$$G_n(s, \theta) = \sum_{k=1}^{n} \psi_k\gamma_k(s) = \Psi_n^T\Gamma_n(s),$$

with $\Psi_n^T = [\psi_1 \;\ldots\; \psi_n]$ and $\Gamma_n(s) = [\gamma_1(s) \;\ldots\; \gamma_n(s)]^T$.

The second step is to find the linear combination of the modes that fits the best to the true frequency response, using the criterion (12) and minimizing over Ψ_n. This is an LS problem and the solution is obtained by solving the corresponding normal equation, see *e.g.* Söderström and Stoica (1989).

In this work $G_n^F(s, \theta_1^F)$ is modeled exactly as described above, which means that its magnitude will have a roll off of second order for high frequencies. However, as is evident from Figure 2 (upper left graph), $\hat{G}^u(\omega)$ is not strictly proper (but still proper). Due to this a feedthrough term is added to $G_n^u(s, \theta_1^u)$, which is easily handled by letting $\Psi_n^T = [\psi_0 \;\psi_1 \;\ldots\; \psi_n]$ and $\Gamma_n(s) = [1 \;\gamma_1(s) \;\ldots\; \gamma_n(s)]^T$ for this case.

4.2 Method 2

Method 2 is used in *e.g.* Moheimani et al. (2003), and is based on modal analysis of the E-B equation (1), see *e.g.* Meirovitch (1997). This approach is based on the assumption that the solution to (1) is separable, and can be written as $w(t, x) = \phi(x)q(t)$, which, when put into (1), leads to an eigenvalue problem. As a consequence of this the solution of (1) can be expressed as the infinite sum

$$w(t, x) = \sum_{k=1}^{\infty} \phi_k(x)q_k(t),$$

where $\phi_k(x)$ are the eigenfunctions for the eigenvalue problem, and the shapes of these depend on the boundary conditions of (1). The eigenfunctions $\phi_k(x)$ are orthogonal, and by exploiting this property the PDE (1) transforms into an infinite number of decoupled second order ODEs in $q(t)$,

$$\ddot{q}_k(t) + \omega_k^2 q(t) = f_k(t), \;\; k = 1, 2, \ldots, \tag{13}$$

where ω_k^2, $k = 1, 2, \dots$ are the eigenvalues, and $f_k(t)$ is the inner product of $f(t,x)$ and $\phi_k(x)$. By taking the Laplace transform of (13) , the solution of (1) can finally be written as

$$W(s,x) = \sum_{k=1}^{\infty} \frac{\phi_k(x)}{s^2 + \omega_k^2} F(s). \tag{14}$$

See Meirovitch (1997) for a thorough analysis of the method.

In Method 2 a finite order model of the system is simply obtained by truncating the infinite sum (14), *i.e.* keep the modes of interest and omit the remaining ones. The advantage is that the resonant modes are expressed explicitly in the sum, but also that the so obtained model is valid for all of the beam — the dependence of the spatial coordinate x remains in the finite order model. This, however, is due to the knowledge of the eigenfunctions $\phi_k(x)$, and explicit expressions for these are easily obtained only for very simple conditions of the beam in terms of geometry, homogeneity etc. As indicated above this modal analysis approach is valid for the elastic case, where the resonant modes are totally undamped.

In a more realistic case, like the one in this study, the method is not applicable unless the system is approximated with a simpler model (w.r.t. geometry, homogeneity etc) for which the modal analysis is more easily performed. To account for damping the denominators in the individual terms in (14) can be complemented with a damping term, so that the denominators become $s^2 + 2\zeta_k\omega_k s + \omega_k^2$, where ζ_k is the damping ratio for mode k. The damping ratios ζ_k then must be chosen in some appropriate way.

In this particular case the following simplifications are made in order to perform the modal analysis: The beam is assumed to be homogeneous, which means that the effect of the actuators, the piezoelectric elements, is neglected. Hence, A, ρ, E and I are assumed to be constant all over the beam. Also, the damping ratios were all set to the same value, $\zeta_k = \zeta$ for all k. Since it is the strain, ϵ, that is measured and regarded as output, rather than the deflection, w, the system will finally be modeled as

$$Y(s) = G_n^u(s, \theta_2^u)U(s) + G_n^F(s, \theta_2^F)F(s) \tag{15}$$

with

$$G_n^u(s, \theta_2^u) = C_u \sum_{k=1}^{n} \frac{\phi(x_s)\left[\phi_k'(x_2) - \phi_k'(x_1)\right]}{s^2 + 2\zeta\omega_k s + \omega_k^2},$$

$$G_n^F(s, \theta_2^F) = C_F \sum_{k=1}^{n} \frac{\phi_k''(x_s)\phi_k(L)}{s^2 + 2\zeta\omega_k s + \omega_k^2},$$

where $x_s = (x_1 + x_2)/2$ as previously, $\phi'(x)$ and $\phi''(x)$ denotes the first and second derivatives of $\phi(x)$ respectively, and C_u and C_F are constants that depend on the geometry and properties of the (simplified) beam — see Norlander (2011) for a derivation.

It should be noted that the natural frequencies ω_k and the constants C_u and C_F are determined by A, ρ, E and I for the *simplified* beam. Since the simplified beam is fictional these properties can be chosen to somehow reflect the corresponding average properties for the actual beam. Here this is exploited to obtain as good fidelity as possible to the true system for low frequencies, including the first resonant mode. More specifically, rather then finding suitable values of A, ρ, E and I explicitly, ω_1 and ζ are chosen to match the first peak in the frequency response with that of the true system, and C_u and C_F are chosen to obtain correct static gains, *i.e.* so that $G_n^u(0, \theta_2^u) = \hat{G}^u(0)$ and $G_n^F(0, \theta_2^F) = \hat{G}^F(0)$. It is stressed that all the natural frequencies depend on A, ρ, E and I, which has the consequence that once ω_1 is chosen, all the other ω_k (for $k = 2, \dots$) are also implicitly determined. Also, the choice of damping ratio ζ will influence all the resonant modes.

4.3 Comparison of models

For a given number of resonant modes, n, both methods provide models of equivalent complexity (*e.g.* model order). However, Method 1 offers more degrees of freedom, *i.e.* more parameters need to be determined, than is the case for Method 2.

In Figure 2 the Bode plots of models with three modes (sixth order models) are shown together with the Bode plot of the true system (10). Since the true system is only known in terms of its frequency response for a finite bandwidth, a model with eleven modes, obtained with Method 1, is used for time simulations of the closed loop systems in Section 5. The magnitude of the absolute model error for this model is also shown in Figure 2.

In the frequency range $0 - 300$ rad/s, the frequency response of the model from Method 1 (referred to as model 1 in the sequel) is barely distinguishable from that of the true system. For the model from Method 2 (referred to as model 2 in the sequel) the frequency response is fairly close to the true system in the F-y-channel, with a slight mismatch of the second and third resonance peaks. In the u-y-channel model 2 has a significant exaggeration of the resonance peaks. This is explained by the adjustment of C_u for a correct static gain in (15).

5. CONTROLLER DESIGN

The purpose of this study is to investigate the effect of the model on the performance of the closed loop system. It is the models 1 and 2, as described in Section 4, that are used for model based control design, and then the corresponding closed loop systems are compared and evaluated. For the controller design the standard linear quadratic Gaussian (LQG) control design technique is employed. More specifically, with the models in state space form as

$$\dot{x}(t) = Ax(t) + Bu(t) + NF(t), \tag{16}$$

$$y(t) = Cx(t) + Du(t) + e(t), \tag{17}$$

the criterion

$$J = E\left[\int_0^\infty \left(Q_1 y(t)^2 + Q_2 u(t)^2\right) dt\right] \tag{18}$$

should be minimized. In the model (16)–(17) $F(t)$ is (as before) the disturbance force, acting at the free end of the beam, and $e(t)$ is the measurement noise. Both these are scalar and are assumed to be random with $E[F(t+\tau)F(t)] = R_1\delta(\tau)$, $E[e(t+\tau)e(t)] = R_2\delta(\tau)$ and $E[F(t+\tau)e(t)] \equiv 0$. The factors $Q_1 \geq 0$ and $Q_2 > 0$ in (18) are weights that can be regarded as design parameters.

The resulting controller is the control law $u(t) = -L\hat{x}(t)$, where $\hat{x}(t)$ is the estimated state vector obtained from the Kalman filter

$$\dot{\hat{x}}(t) = A\hat{x}(t) + Bu(t) + K(y(t) - C\hat{x}(t) - Du(t)). \tag{19}$$

The feedback gain L (not to be confused with the beam length) is a row vector which depends on the ratio Q_1/Q_2. The Kalman gain K is a column vector which depends on the ratio R_1/R_2. Obviously L and K also depend on the model (16)–(17).

See standard textbooks, *e.g.* Goodwin et al. (2001) and Glad and Ljung (2000), for more details on LQG control design.

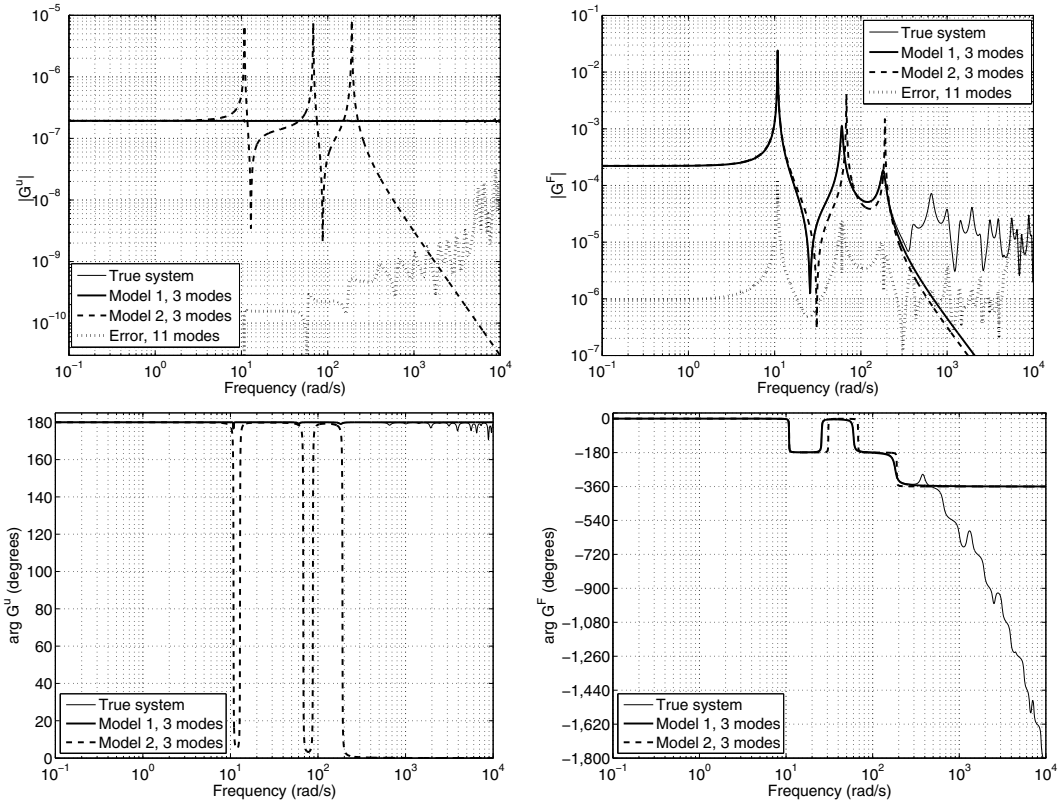

Fig. 2. Bode plots of the true system and the models obtained by Methods 1 and 2 with 3 modes. Upper and lower graphs shows the magnitude and the phase respectively, the left and right graphs shows the $U-y$- and $F-y$-channels respectively. The upper plots also show the magnitude of the absolute model error for the model with eleven modes, obtained with Method 1.

The main control objective is to reduce vibrations due to the disturbance force F in the frequency range 0–300 rad/s, or, put in another way, to dampen out the three first resonance peaks.

In order to handle the vast difference in magnitude of the involved signals, these were scaled according to

$$u = D_u u_s, \;\; y = D_y y_s, \;\; \text{and } F = \; D_F F_s, \qquad (20)$$

and the following scalings were used:

$$D_u = 250, \;\; D_y = 10^{-4} \;\text{ and } D_F = 1. \qquad (21)$$

The controllers computed depend on Q_1, Q_2, R_1 and R_2 (which can be regarded as design parameters), and on the model used in the design. Here it is the effect of the *model* that is investigated, so for the two models identical sets of Q_1, Q_2, R_1 and R_2 are used. Two cases are considered, denoted case (a) and (b). For both cases the parameters $Q_1 = 1$, $Q_2 = 0.001$ and $R_1 = 1$ are used — only R_2 differs, according to

$$\text{case (a): } \; R_2 = 1, \;\; \text{case (b): } \; R_2 = 0.01.$$

The choice of Q_1 and Q_2 is considered as a reasonable balance between disturbance attenuation and control effort, while R_1 is motivated by the scaling of F as described above. It is considered as a realistic scenario that the measurement noise is of the same magnitude as the measured output y, or slightly less. This motivates these choices of R_2.

In total there are four controllers, referred to as controller 1a, 1b, 2a and 2b, indicating that they are based on model 1 or 2, and for case (a) or (b) respectively.

6. EVALUATION OF THE CONTROLLERS

The four controllers are evaluated on the true system, in the sense that the frequency responses of the corresponding closed loop systems are computed (remember that the frequency response of the true system is known). In particular the response from the disturbance force F to the strain y is of interest, as it shows how well the disturbance is attenuated by the controllers. This closed loop system can be represented by $Y(s) = G^F(s)S(s)F(s)$, where

$$S(s) = \frac{1}{1 + C(s)G^u(s)},$$

is the sensitivity function. Here $C(s)$ is the transfer function of the controller, and $G^u(s)$ and $G^F(s)$ are the presumed transfer functions for the cantilever beam. The magnitude plots for $G^F(s)S(s)$ are shown in Figures 3 and 4 for the cases (a) and (b) respectively. The frequency response $\hat{G}^F(\omega)$ is also shown, for comparison.

Simulations of the impulse responses of $G^F(s)S(s)$ for all four controllers have also been performed. The impulse responses for case (b) are shown in Figure 5. The impulse response of $G^F(s)$, *i.e.* the open loop system, is also shown for comparison. Note that the time axis has a logarithmic scale. This rather unorthodox convention is used merely to be able to visualize the behavior in different time scales in one plot only. For these simulations the model with eleven modes was used.

From Figures 3 and 4 it is clear that the controllers 1a and 1b performs better than the controllers 2a and 2b *in the intended frequency range*, *i.e.* up to 300 rad/s, including the three

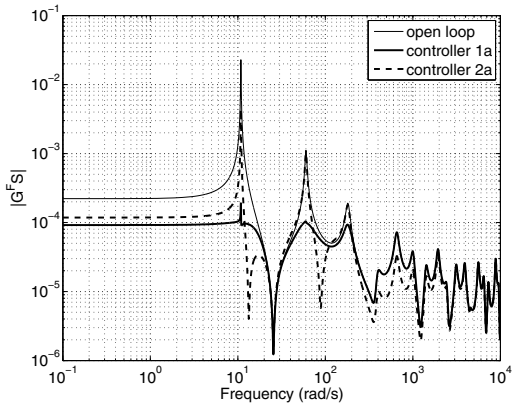

Fig. 3. The magnitude of the frequency response from F to y for the open and closed loop systems for case (a), *i.e.* $R_2 = 1$.

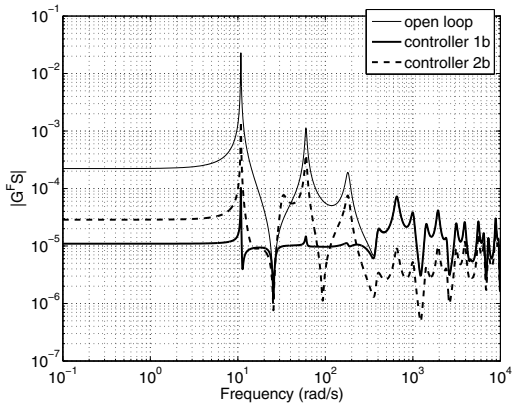

Fig. 4. The magnitude of the frequency response from F to y for the open and closed loop systems for case (b), *i.e.* $R_2 = 0.01$.

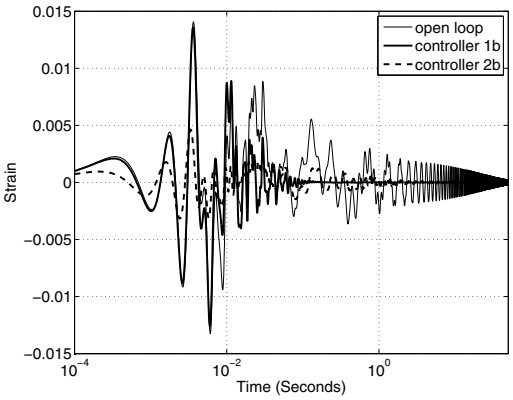

Fig. 5. Impulse responses from F to y for case (b).

first resonant modes. For frequencies higher than 300 rad/s $|G^F(i\omega)S(i\omega)|$ coincides with $|G^F(i\omega)|$ for the controllers 1a and 1b. It is interesting though that the controllers 2a and 2b do have disturbance attenuation for frequencies higher than 300 rad/s and thus perform better than the controllers 1a and 1b in that range, and particularly so in case (b).

The impulse response simulations support these results, see Figure 5. The controllers 1a and 1b dampen out the oscillations within the first few tenths of a second, while the controllers 2a and 2b need several seconds to dampen the oscillations out. This is still a considerable improvement compared to the open loop system, which continuous to oscillate for 100 seconds and more. On the other hand, looking at the very first part of the impulse response the controllers 1a and 1b have no effect until after circa 0.01 seconds, but the controllers 2a and 2b actually attenuates the oscillations slightly from the start already. This is in line the high frequency attenuation for controller 2 observed in the magnitude plots, as discussed above.

A quantitative measure of the disturbance attenuation achieved with the different controllers is the H_2-norm of $G^F(s)S(s)$. The computed values of $||G^F(s)S(s)||_2$ are $9.3 \cdot 10^{-4}$ and $7.4 \cdot 10^{-4}$ for the controllers 1a and 1b, and $1.7 \cdot 10^{-3}$ and $6.3 \cdot 10^{-4}$ for the controllers 2a and 2b respectively. For the open loop system $||G^F(s)||_2 = 5.2 \cdot 10^{-3}$. In the case (a) controller 1 is the most successful, but in case (b) it is instead controller 2 that has the lowest H_2-norm. The reason for that is the better attenuation for controller 2b in the frequency range above 300 rad/s. Still, it could be argued that controller 1b "does the job" better in the intended frequency range (up to 300 rad/s).

7. CONCLUSIONS

The main conclusion of this study is that it *is* worthwhile to endeavor a high accuracy for models used for model based control in order to achieve a good performance. Another conclusion is that Method 2 is functional for producing models for control design, but that a limited control performance should be expected.

REFERENCES

T. Glad and L. Ljung. *Control Theory*. Taylor and Francis, 2000.

G. C. Goodwin, S. F. Graebe, and M. E. Salgado. *Control System Design*. Prentice-Hall, Inc., 2001.

L. Hillström. *Estimation of state and identification of complex modulus based on measurements on a bar traversed by waves*. PhD thesis, Department of Materials Science, Uppsala University, 2001.

L. Hillström, U. Valdek, and B. Lundberg. Estimation of the state vector and identification of the complex modulus of a beam. *Journal of Sound and Vibration*, 261:653–673, 2003.

L. Meirovitch. *Principles and Techniques of Vibration*. Prentice-Hall, Inc., 1997.

S. O. R. Moheimani, D. Halim, and A. J. Fleming. *Spatial Control of Vibration: Theory and Experiments*. World Scientific Publishing Co. Pte. Ltd., 2003.

P. Nauclér, H. Norlander, A. Jansson, and T. Söderström. Modeling and control of a viscoelastic piezolaminated beam. In *Proceedings of the 16th IFAC World Congress*, Prague, Czech Republic, July 2005.

H. Norlander. On the impact of model accuracy for active damping of a viscoelastic beam. Technical Report 2011-013, Department of Information Technology, Uppsala University, 2011.

T. Söderström and P. Stoica. *System Identification*. Prentice–Hall International, 1989.